

 Open access • Posted Content • DOI:10.1101/021592

Salmon provides accurate, fast, and bias-aware transcript expression estimates using dual-phase inference — [Source link](#)





Rob Patro, Geet Duggal, Michael I. Love, Rafael A. Irizarry ...+1 more authors

Institutions: Stony Brook University, Harvard University, Dana Corporation, Carnegie Mellon University

Published on: 30 Aug 2016 - bioRxiv (Cold Spring Harbor Laboratory)

Related papers:

- [Near-optimal probabilistic RNA-seq quantification](#)
- [edgeR: a Bioconductor package for differential expression analysis of digital gene expression data.](#)
- [STAR: ultrafast universal RNA-seq aligner](#)
- [Moderated estimation of fold change and dispersion for RNA-seq data with DESeq2](#)
- [RSEM: accurate transcript quantification from RNA-Seq data with or without a reference genome](#)

Share this paper:    

View more about this paper here: <https://typeset.io/papers/salmon-provides-accurate-fast-and-bias-aware-transcript-39j4qcbf85>

Salmon provides accurate, fast, and bias-aware transcript expression estimates using dual-phase inference

Rob Patro^{*1}, Geet Duggal^{†2}, Michael I Love^{‡3}, Rafael A Irizarry^{§3}, and
Carl Kingsford^{¶4}

¹Department of Computer Science, Stony Brook University

²DNANexus, 1975 W El Camino Real, Suite 101 Mountain View, CA 94040

³Department of Biostatistics and Computational Biology, Dana-Farber Cancer Institute, Department of Biostatistics, Harvard TH Chan School of Public Health

⁴Computational Biology Department, Carnegie Mellon University

August 29, 2016

We introduce *Salmon*, a new method for quantifying transcript abundance from RNA-seq reads that is highly-accurate and very fast. *Salmon* is the first transcriptome-wide quantifier to model and correct for fragment GC content bias, which we demonstrate substantially improves the accuracy of abundance estimates and the reliability of subsequent differential expression analysis compared to existing methods that do not account for these biases. *Salmon* achieves its speed and accuracy by combining a new

^{*}rob.patro@cs.stonybrook.edu

[†]gduggal@dnanexus.com, work done while GD was at CMU.

[‡]mlove@jimmy.harvard.edu

[§]rafa@jimmy.harvard.edu

[¶]carlk@cs.cmu.edu

dual-phase parallel inference algorithm and feature-rich bias models with an ultra-fast read mapping procedure. These innovations yield both exceptional accuracy and order-of-magnitude speed benefits over alignment-based methods.

Estimating transcript abundance across cell types, species, and conditions is a fundamental task in genomics. For example, these estimates are used for the classification of diseases and their subtypes [1], for understanding expression changes during development [2], and tracking the progression of cancer [3]. Accurate and efficient quantification of transcript abundance from RNA-seq data is an especially pressing problem due to both the wide range of technical biases that affect the RNA-seq fragmentation, amplification and sequencing process [4, 5] and the exponentially increasing number of experiments and the growing adoption of expression data for medical diagnosis [6]. Traditional quantification algorithms — those that make use of full alignments of the sequencing reads to the genome or transcriptome to compute abundances — require significant computational resources [7] and do not scale well with the rate at which data is produced [8]. Addressing the efficiency problem has been the focus of much recent work in the area of transcript-level quantification. For example, the quantification tool *Sailfish* [9] achieved an order of magnitude speed improvement over previous approaches by replacing traditional read alignment with the allocation of exact k-mers to transcripts but can sometimes produce less accurate estimates for paired-end data or for stranded protocols. The recently-introduced quantification tool, *kallisto* [10], achieves similar speed improvements and further reduces the gap in accuracy with traditional alignment-based methods by replacing the k-mer counting approach used in *Sailfish* with a procedure called pseudoalignment. Unlike pseudoalignment, *Salmon*'s lightweight mapping procedure tracks the position and orientation of all mapped fragments, and in conjunction with the abundances learned in the online phase of the inference algorithm, makes use of per-fragment conditional probabilities to estimate auxiliary models, bias terms, and aggregate weights for its rich equivalence classes.

However, existing methods for transcriptome-wide abundance estimation, including both traditional, alignment-based approaches and the recently-introduced ultra-fast methods, lack

sample-specific bias models rich enough to capture many of the important effects, like fragment GC content bias, that are observed in experimental data and that can lead to, for example, unacceptable false positive rates in differential expression studies [5].

Our novel quantification procedure called *Salmon* (**Supplementary Fig. 1**) achieves best-in-class accuracy, employs high-fidelity, sample-specific bias models, and simultaneously achieves the same order-of-magnitude speed benefits as *kallisto* and *Sailfish*. Using experimental data from the GEUVADIS [11] and SEQC [28] studies as well as synthetic data from both the *Polyester* [13] and *RSEM-sim* [14] simulators, we benchmark *Salmon* against both *kallisto* [10] (as representative of a state-of-the-art alignment-free method) and *eXpress* [15] + *Bowtie2* [16] (as representative of a state-of-the-art alignment-based method); both of these methods also implement their own bias models. We show that *Salmon* typically outperforms both *kallisto* and *eXpress* in terms of accuracy (**Fig. 1a-d, Supplementary Fig. 4**), often by a substantial margin.

Further, *Salmon*'s dual-phase inference algorithm and rich bias models yield considerably improved inter-replicate concordance (**Supplementary Fig. 2**) compared to both *kallisto* and *eXpress*. For example, when used for differential expression (DE) testing, the quantification estimates produced by *Salmon* exhibit markedly higher sensitivity at the same false discovery rate than those produced by *kallisto* or *eXpress* (**Table 1C**) — achieving a sensitivity 53% to 250% higher, at the same FDRs, compared with existing methods. Likewise, *Salmon* produces fewer false-positive differential expression calls in comparisons that are expected to contain few true differences in transcript expression (**Table 1D**). These benefits of *Salmon* over other methods persist in gene-level analysis as well, where the use of *Salmon*'s estimates for gene-level DE analysis leads to a decrease by a factor of ~ 2.6 in the number of genes that are called as DE (**Supplementary Table 1**). **Supplementary Fig. 5** shows specific examples from the GEUVADIS experiments where dominant isoform switching is observed ($p < 1 \times 10^{-6}$) between samples under the quantification estimates produced by *kallisto* or *eXpress*, but this isoform switching is eliminated under the abundance estimates of *Salmon* that account for fragment GC bias. In idealized simulations, like those generated by *RSEM-sim*, where realistic biases are not simulated,

the accuracy estimates of different methods tend to be more similar to one another (**Fig. 1b, Supplementary Fig. 6**). These idealized *RSEM-sim* simulation results, where the fragments are generated without bias and in perfect accordance with the generative model adopted by the quantifiers, serve as a useful measure of the internal consistency of the algorithms and have been used in other validation contexts [14, 10]. However, we expect our results on the SEQC [28], GEUVADIS [11], and *Polyester* [13] (simulated with bias) data sets to be more representative of typical real-world performance.

Salmon incorporates a rich model of experimental biases, which allows it to account for the effects of sample-specific parameters and biases that are typical of RNA-seq data, including positional biases in coverage, sequence-specific biases at both the 5' and 3' end of sequenced fragments, fragment-level GC bias, strand-specific protocols, and the fragment length distribution. These biases are automatically learned in the online phase of the algorithm, and are encoded in a fragment-transcript agreement model (**Online methods, Fragment-transcript agreement model**). In this model, fragment-transcript assignment scores are defined as proportional to (1) the chance of observing a fragment length given a particular transcript/isoform of a gene, (2) the chance that a fragment starts at a particular position on the transcript, (3) the concordance of the fragment aligning with a user-defined sequencing library format (e.g. a paired ended, stranded protocol), and (4) the chance that the fragment came from the transcript based on a score obtained from the alignment procedure (if alignments are being used). Additionally, based on the computed mappings, *Salmon* gathers information about the positional, sequence-specific and fragment GC content of the observed fragments. *Salmon* incorporates these biases and experimental parameters by learning auxiliary models that describe the relevant distributions and maintaining 'rich equivalence classes' of fragments (**Online methods, Equivalence classes**) that act as an efficient representation of the sequenced fragments during the offline inference phase and speed up the process of estimating transcript abundances.

Salmon's two-phase, parallel inference procedure consists of both a streaming, online inference phase, where estimates of transcript abundance are continuously updated after

considering each small batch of reads, and an offline inference phase that operates over a highly-reduced representation of the sequencing experiment (**Online methods, Online phase and Offline phase**; Illustration of method in **Supplementary Fig. 1**). This two-phase inference procedure allows *Salmon* to build a probabilistic model of the sequencing experiment that incorporates information not considered by *Sailfish* [9] and *kallisto* [10]. During the online inference phase, *Salmon* learns and continuously updates transcript-level abundance estimates. In turn, this allows the evaluation of per-fragment probabilities that are not directly represented in the factorized likelihood function (**Offline phase**). These probabilities enable accounting, proportionally, for all of the potential mapping locations of a fragment when estimating experiment and bias model parameters.

Salmon is designed take advantage of multiple CPU cores, and the mapping and inference procedures scale well with the number of reads in an experiment. *Salmon* can quantify abundance either via a builtin, ultra-fast read-mapping procedure [17], or using pre-computed alignments provided in SAM or BAM format. This approach allows *Salmon* to achieve high accuracy while maintaining a speed similar to that of *kallisto* [10]. For example, *Salmon* can quantify a data set of approximately 600 million reads (75bp, paired-end) in 23 minutes using 30 threads — this roughly matches the speed of the recently-introduced *kallisto*, which took 20 minutes to complete the same task (wall clock time on a 24 core (with hyperthreading) machine with 256Gb of RAM. Each core is Intel[®] Xeon[®] CPU (E5-4607 v2 2.60GHz).

The simultaneous speed and accuracy of *Salmon* is achieved using the dual-phase approach described above together with quasi-mapping [17]. Therefore, *Salmon* encompasses both the “alignment” and “quantification” phases that are required by more traditional quantification pipelines in a single tool. A quasi-mapping represents a match between a sequenced fragment and a transcript and consists of a tuple $m_i = (t, p_\ell, p_r, o_\ell, o_r)$ containing the transcript t to which the fragment maps, the positions p_ℓ, p_r where the left and right ends of the fragment map, and the orientations o_ℓ, o_r with which the fragment ends map, but not the nucleotide-to-nucleotide correspondence between the fragment and transcript. When run in quasi-mapping mode, *Salmon*

takes as input an index of the transcriptome and a set of *raw* sequencing reads (i.e. unaligned reads in FASTA/Q format) and performs quantification directly without generating any intermediate alignment files. This saves considerable time and space, since quasi-mapping is considerably faster than traditional alignment. Thus, while *Salmon* is also capable of performing quantification using existing alignments of a sequencing experiment to the transcriptome, if a users prefers to provide these, we anticipate that *Salmon* will be primarily used in quasi-mapping mode.

Salmon's approach is unique in the way that it combines useful models of experimental data with an efficient parallel inference procedure. This combination has produced some of the most accurate expression estimates to date without sacrificing the order of magnitude speed improvements enjoyed by recent approaches (e.g. [9], [10]). *Salmon*'s ability to compute high-quality estimates of transcript abundances at the scale of thousands of samples, while also accounting for the prevalent technical biases affecting transcript quantification [18], will enable individual expression experiments to be interpreted in the context of many rapidly growing sequence expression databases. This will allow for a more comprehensive comparison of the similarity of experiments across large populations of individuals and across different environmental conditions and cell types. *Salmon* is open-source and freely-licensed (GPLv3). It is written in C++11, and is available at <https://github.com/COMBINE-lab/salmon>.

Acknowledgements

This research is funded in part by the Gordon and Betty Moore Foundation's Data- Driven Discovery Initiative through Grant GBMF4554 to C.K. It is partially funded by the US National Science Foundation (CCF-1256087, CCF-1319998, BBSRC-NSF/BIO-1564917) and the US National Institutes of Health (R21HG006913, R01HG007104). C.K. received support as an Alfred P. Sloan Research Fellow. This work was partially completed while G.D. was a postdoctoral fellow in the Computational Biology Department at Carnegie Mellon University.

M.L. was supported by NIH grant 5T32CA009337-35. R.I. was supported by NIH R01 grant HG005220.

Author Contributions R.P. and C.K. designed the method, which was implemented by R.P. R.P., G.D., M.L., R.I. and C.K. designed the experiments and R.P., G.D. and M.L. conducted the experiments. R.P., G.D., M.L., R.I. and C.K. wrote the manuscript.

References

- [1] Katherine A Hoadley, Christina Yau, Denise M Wolf, Andrew D Cherniack, David Tamborero, Sam Ng, Max DM Leiserson, Beifang Niu, Michael D McLellan, Vladislav Uzunangelov, et al. Multiplatform analysis of 12 cancer types reveals molecular classification within and across tissues of origin. *Cell*, 158(4):929–944, 2014.
- [2] Jingyi Jessica Li, Haiyan Huang, Peter J Bickel, and Steven E Brenner. Comparison of *D. melanogaster* and *C. elegans* developmental stages, tissues, and cells by modENCODE RNA-seq data. *Genome Research*, 24(7):1086–1101, 2014.
- [3] John N Weinstein, Eric A Collisson, Gordon B Mills, Kenna R Mills Shaw, Brad A Ozenberger, Kyle Ellrott, Ilya Shmulevich, Chris Sander, Joshua M Stuart, Cancer Genome Atlas Research Network, et al. The cancer genome atlas pan-cancer analysis project. *Nature Genetics*, 45(10):1113–1120, 2013.
- [4] Adam Roberts, Cole Trapnell, Julie Donaghey, John L Rinn, Lior Pachter, et al. Improving RNA-Seq expression estimates by correcting for fragment bias. *Genome Biology*, 12(3):R22, 2011.
- [5] Michael I Love, John B Hogenesch, and Rafael A Irizarry. Modeling of RNA-seq fragment sequence bias reduces systematic errors in transcript abundance estimation. *bioRxiv*, page 025767, 2015.

- [6] Ignasi Morán, İldem Akerman, Martijn van de Bunt, Ruiyu Xie, Marion Benazra, Takao Nammo, Luis Arnes, Nikolina Nakić, Javier García-Hurtado, Santiago Rodríguez-Seguí, et al. Human β cell transcriptome analysis uncovers lncRNAs that are tissue-specific, dynamically regulated, and abnormally expressed in type 2 diabetes. *Cell Metabolism*, 16(4):435–448, 2012.
- [7] Mingxiang Teng, Michael I Love, Carrie A Davis, Sarah Djebali, Alexander Dobin, Brenton R Graveley, Sheng Li, Christopher E Mason, Sara Olson, Dmitri Pervouchine, et al. A benchmark for RNA-seq quantification pipelines. *Genome biology*, 17(1):1, 2016.
- [8] Yuichi Kodama, Martin Shumway, and Rasko Leinonen. The Sequence Read Archive: explosive growth of sequencing data. *Nucleic Acids Research*, 40(D1):D54–D56, 2012.
- [9] Rob Patro, Stephen M Mount, and Carl Kingsford. Sailfish enables alignment-free isoform quantification from RNA-seq reads using lightweight algorithms. *Nature Biotechnology*, 32(5):462–464, 2014.
- [10] Nicolas L Bray, Harold Pimentel, Páll Melsted, and Lior Pachter. Near-optimal probabilistic RNA-seq quantification. *Nature Biotechnology*, 34(5):525–527, 2016.
- [11] Tuuli Lappalainen, Michael Sammeth, Marc R Friedländer, Peter A. C. ’t Hoen, Jean Monlong, Manuel A Rivas, Mar González-Porta, Natalja Kurbatova, Thasso Griebel, Pedro G Ferreira, et al. Transcriptome and genome sequencing uncovers functional variation in humans. *Nature*, 501(7468):506–511, 2013.
- [12] SEQC/MAQC-III Consortium et al. A comprehensive assessment of RNA-seq accuracy, reproducibility and information content by the Sequencing Quality Control Consortium. *Nature Biotechnology*, 32(9):903–914, 2014.
- [13] Alyssa C Frazee, Andrew E Jaffe, Ben Langmead, and Jeffrey T Leek. Polyester: simulating RNA-seq datasets with differential transcript expression. *Bioinformatics*, 31(17):2778–2784, 2015.

- [14] Bo Li, Victor Ruotti, Ron M Stewart, James A Thomson, and Colin N Dewey. RNA-Seq gene expression estimation with read mapping uncertainty. *Bioinformatics*, 26(4):493–500, 2010.
- [15] Adam Roberts and Lior Pachter. Streaming fragment assignment for real-time analysis of sequencing experiments. *Nature Methods*, 10(1):71–73, 2013.
- [16] Ben Langmead and Steven L Salzberg. Fast gapped-read alignment with Bowtie 2. *Nature Methods*, 9(4):357–359, 2012.
- [17] Avi Srivastava, Hirak Sarkar, Nitish Gupta, and Rob Patro. RapMap: a rapid, sensitive and accurate tool for mapping RNA-seq reads to transcriptomes. *Bioinformatics*, 32(12):i192–i200, 2016.
- [18] Peter A. C. ’t Hoen, Marc R Friedländer, Jonas Almlöf, Michael Sammeth, Irina Pulyakhina, Seyed Yahya Anvar, Jeroen FJ Laros, Henk PJ Buermans, Olof Karlberg, Mathias Brännvall, et al. Reproducibility of high-throughput mRNA and small RNA sequencing across laboratories. *Nature biotechnology*, 31(11):1015–1022, 2013.

Figure 1

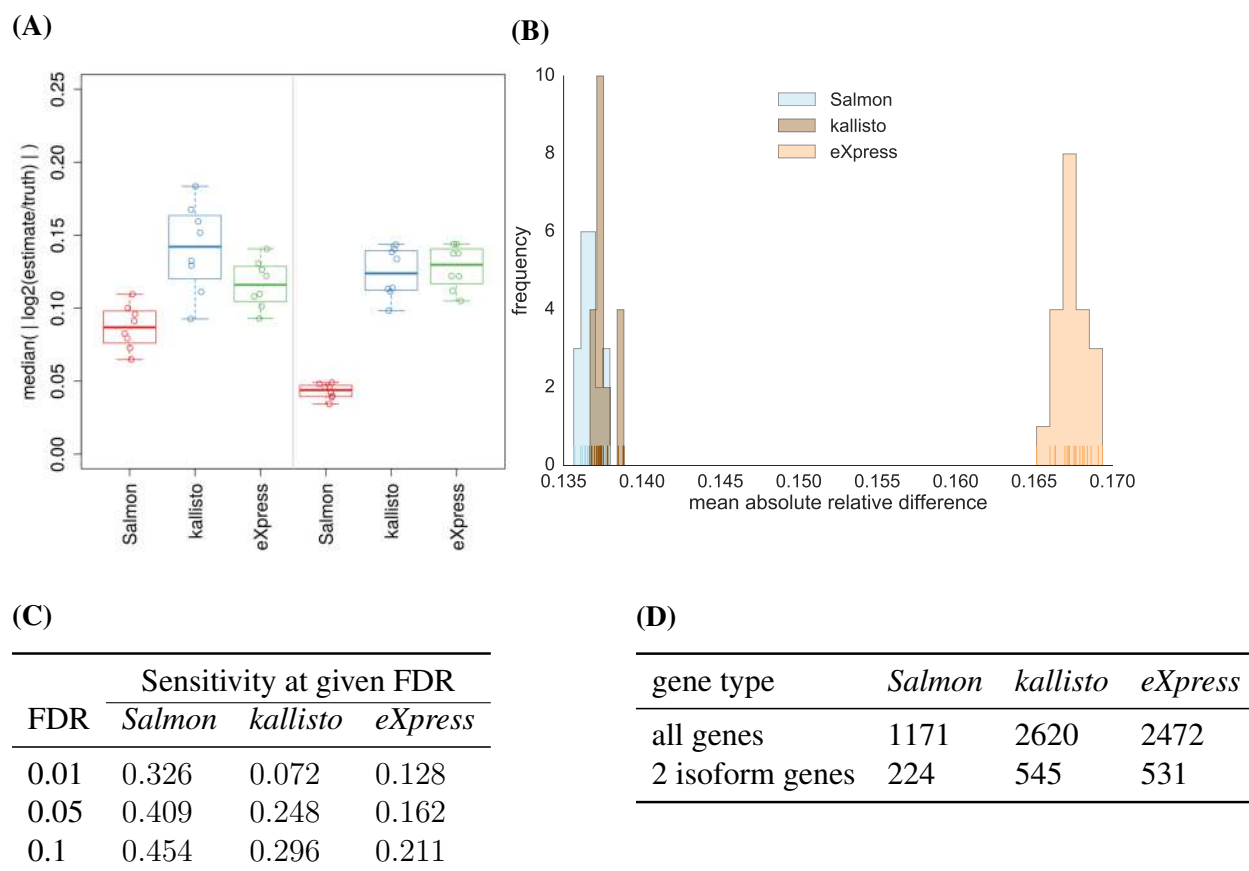


Figure 1: (A) The median of absolute log fold changes (lfc) between the estimated and true abundances under all 16 replicates of the *Polyester* simulated data. The closer the lfc to zero, the more similar the true and estimated abundances. The left and right panels show the distribution of the log fold changes under samples simulated with different GC-bias curves learned from experimental data (details in **Online methods, Ground truth simulated data**). (B) The distribution of mean absolute relative differences (MARDs), as described in **Online methods, Metrics for accuracy**, of *Salmon*, *kallisto* and *eXpress* under 20 simulated replicates generated by *RSEM-sim*. *Salmon* and *kallisto* yield similar MARDs, though *Salmon*'s distribution of MARDs is significantly smaller (Mann-Whitney U test, $p = 0.00017$) than those of *kallisto*. Both methods outperform *eXpress* (Mann-Whitney U test, $p = 3.39781 \times 10^{-8}$). (C) At typical FDR values, the sensitivity of finding truly DE transcripts using *Salmon*'s estimates is 53% – 450% greater than that using *kallisto*'s estimates and 210% – 250% greater than that using *eXpress*' estimates for the *Polyester* simulated data. (D) For 30 GEUVADIS samples, the number of transcripts called as DE at an expected FDR of 1% when the contrast between groups is simply a technical confound (i.e. the center at which they were sequenced). *Salmon* produces fewer than half as many DE calls as the other methods.

Online methods

Objectives and models for abundance estimation

Our main goal is to quantify, given a known transcriptome \mathcal{T} and a set of sequenced fragments \mathcal{F} , the relative abundance of each transcript in our input sample. This problem is challenging both statistically and computationally. The main statistical challenges derive from need to resolve a complex and often very high-dimensional mixture model (i.e. estimating the relative abundances of the transcripts given the collection of ambiguously mapping sequenced fragments). The main computational challenges derive from the need to process datasets that commonly consist of tens of millions of fragments, in conditions where each fragment might reasonably map to many different transcripts. We lay out below how we tackle these challenges, beginning with a description of our assumed generative model of the sequencing experiment, upon which we will perform inference to estimate transcript abundances.

We also make note of the notation we use in the methods described below. Here, we use the vertical bar $|$ to indicate that the fixed quantities following are parameters used to calculate the probability. For the Bayesian objective, the notation implies conditioning on these random variables.

Generative process Assume that, for a particular sequencing experiment, the underlying true transcriptome is given as $\mathcal{T} = \{(t_1, \dots, t_M), (c_1, \dots, c_M)\}$, where each t_i is the nucleotide sequence of some transcript (an isoform of some gene) and each c_i is the corresponding number of copies of t_i in the sample. Further, we denote by ℓ_i the length of transcript t_i and by $\tilde{\ell}_i$ the *effective length* of transcript t_i , as defined in Equation (1). We adopt a generative model of the sequencing experiment that dictates that, in the absence of experimental bias, library fragments are sampled proportional to $c_i \cdot \tilde{\ell}_i$. That is, the probability of drawing a sequencing fragment from some position on a particular transcript t_i is proportional the total fraction of all nucleotides in the

sample that originate from a copy of t_i . This quantity is called the nucleotide fraction [14]:

$$\eta_i = \frac{c_i \cdot \tilde{\ell}_i}{\sum_{j=1}^M c_j \cdot \tilde{\ell}_j}.$$

The true nucleotide fractions, η , though not directly observable, would provide us with a way to measure the true relative abundance of each transcript in our sample. Specifically, if we normalize the η_i by the effective transcript length $\tilde{\ell}_i$, we obtain a quantity

$$\tau_i = \frac{\frac{\eta_i}{\tilde{\ell}_i}}{\sum_{j=1}^M \frac{\eta_j}{\tilde{\ell}_j}},$$

called the transcript fraction [14]. These τ can be used to immediately compute common measures of relative transcript abundance like transcripts per million (TPM). The TPM measure for a particular transcript is the number of copies of this transcript that we would expect to exist in a collection of one million transcripts, assuming this collection had exactly same distribution of abundances as our sample. The TPM for transcript t_i , is given by $\text{TPM}_i = \tau_i 10^6$. Of course, in a real sequencing experiment, there are numerous biases and sampling effects that may alter the above assumptions, and accounting for them is essential for accurate inference. Below we describe how *Salmon* accounts for 5' and 3' sequence-specific biases (which are not considered separately by *kallisto*) and fragment GC bias which is modeled by neither *kallisto* nor *eXpress*.

Effective length A transcript's effective length depends on the empirical fragment length distribution of the underlying sample and the length of the transcript. It accounts for the fact that the range of fragment sizes that can be sampled is limited near the ends of a transcript. Here, fragments refer to the (potentially size-selected) cDNA fragments of the underlying library, from the ends of which sequencing reads are generated. In paired-end data, the mapping positions of the reads can be used to infer the empirical distribution of fragment lengths in the underlying library, while the expected mean and standard deviation of this distribution must be provided for single-end libraries. We compute the effective transcript lengths using the approach of [10],

which defines the effective length of a transcript t_i as

$$\tilde{\ell}_i = \ell_i - \mu_d^{\ell_i}, \quad (1)$$

where $\mu_d^{\ell_i}$ is the mean of the truncated empirical fragment length distribution. Specifically, let d be the empirical fragment length distribution, and $\Pr\{X = x\}$ be the probability of drawing a fragment of length x under d , then $\mu_d^{\ell_i} = \sum_{j=1}^{\ell_i} j \cdot \Pr\{X = j\} / \sum_{k=1}^{\ell_i} \Pr\{X = k\}$.

Given a collection of observations (raw sequenced fragments or alignments thereof), and a model similar to the one described above, there are numerous approaches to inferring the relative abundance of the transcripts in the target transcriptome, \mathcal{T} . Here we describe two basic inference schemes, both available in *Salmon*, which are commonly used to perform inference in such a model. All of the results reported in the manuscript were computed using the maximum likelihood objective (i.e. the EM algorithm) in the offline phase, which is the default in *Salmon*.

Maximum likelihood objective

The first scheme takes a maximum likelihood approach to solving for the quantities of interest. Specifically, if we assume that all fragments are generated independently, and we are given a vector of known nucleotide fractions $\boldsymbol{\eta}$, a binary matrix of transcript-fragment assignment \mathbf{Z} where $z_{ji} = 1$ if fragment j is derived from transcript i , and the set of transcripts \mathcal{T} , we can write the probability of observing a set of sequenced fragments \mathcal{F} as:

$$\Pr\{\mathcal{F} \mid \boldsymbol{\eta}, \mathbf{Z}, \mathcal{T}\} = \prod_{j=1}^N \Pr\{f_j \mid \boldsymbol{\eta}, \mathbf{Z}, \mathcal{T}\} = \prod_{j=1}^N \sum_{i=1}^M \Pr\{t_i \mid \boldsymbol{\eta}\} \cdot \Pr\{f_j \mid t_i, z_{ji} = 1\}. \quad (2)$$

Where $|\mathcal{F}| = N$ is the number of sequenced fragments, $\Pr\{t_i \mid \boldsymbol{\eta}\}$ is the probability of selecting transcript t_i to generate some fragment given the nucleotide fraction $\boldsymbol{\eta}$, and we have that $\Pr\{t_i \mid \boldsymbol{\eta}\} = \eta_i$. $\Pr\{f_j \mid t_i, z_{ji} = 1\}$ is the probability of generating fragment j given that it came from transcript i . We will use $\Pr\{f_j \mid t_i\}$ as shorthand for $\Pr\{f_j \mid t_i, z_{ji} = 1\}$ since $\Pr\{f_j \mid t_i, z_{ji} = 0\}$ is uniformly 0. The determination of $\Pr\{f_j \mid t_i\}$ is defined in further detail

in **Fragment-transcript agreement model**. The likelihood associated with this objective can be optimized using the EM algorithm as in [14].

Bayesian objective

One can also take a Bayesian approach to transcript abundance inference as done in [19, 20]. In this approach, rather than directly seeking maximum likelihood estimates of the parameters of interest, we want to infer the posterior distribution of $\boldsymbol{\eta}$. In the notation of [19], we wish to infer $\Pr\{\boldsymbol{\eta} \mid \mathcal{F}, \mathcal{T}, \mathcal{Z}\}$ — the posterior distribution of nucleotide fractions given the transcriptome \mathcal{T} and the observed fragments \mathcal{F} . This distribution can be written as:

$$\Pr\{\boldsymbol{\eta} \mid \mathcal{F}, \mathcal{T}, \mathcal{Z}\} \propto \sum_{\mathbf{Z} \in \mathcal{Z}} \Pr\{\mathcal{F} \mid \mathcal{T}, \mathbf{Z}\} \cdot \Pr\{\mathbf{Z} \mid \boldsymbol{\eta}\} \cdot \Pr\{\boldsymbol{\eta}\}, \quad (3)$$

where

$$\Pr\{\mathbf{Z} \mid \boldsymbol{\eta}\} = \prod_{i=1}^M \prod_{j=1}^N \eta_j^{z_{ji}}, \quad (4)$$

and

$$\Pr\{\mathcal{F} \mid \mathcal{T}, \mathbf{Z}\} = \prod_{i=1}^M \prod_{j=1}^N \Pr\{f_j \mid t_i\}^{z_{ji}}. \quad (5)$$

Unfortunately, direct inference on the distribution $\Pr\{\boldsymbol{\eta} \mid \mathcal{F}, \mathcal{T}, \mathcal{Z}\}$ is intractable because its evaluation requires the summation over the exponentially large latent variable configuration space \mathcal{Z} . Since the posterior distribution cannot be directly estimated, we must rely on some form of approximate inference. One particularly attractive approach is to apply variational Bayesian (VB) inference in which some tractable approximation to the posterior distribution is assumed.

Subsequently, one seeks the parameters for the approximate posterior under which it best matches the true posterior. Essentially, this turns the inference problem into an optimization problem — finding the optimal set of parameters — which can be efficiently solved by a number of different algorithms. In particular, variational inference seeks to find the parameters for the approximate posterior that minimizes the Kullback-Leibler (KL) divergence between the

approximate and true posterior distribution. Though the true posterior may be intractable, this minimization can be achieved by maximizing a lower-bound on the marginal likelihood of the posterior distribution [21], written in terms of the approximate posterior. *Salmon* optimizes the collapsed variational Bayesian objective [19] in its online phase and the full variational Bayesian objective [20] in the variational Bayesian mode of its offline phase (see **Offline phase**).

Fragment-transcript agreement model

We model the conditional probability $\Pr\{f_j \mid t_i\}$ for generating f_j given t_i using a number of auxiliary terms. These terms come from auxiliary models whose parameters do not explicitly depend upon the current estimates of transcript abundances. Thus, once the parameters of these models have been learned and are fixed, these terms do not change even when the estimate for $\Pr\{t_i \mid \boldsymbol{\eta}\} = \eta_i$ needs to be updated. *Salmon* uses the following auxiliary terms:

$$\Pr\{f_j \mid t_i\} = \Pr\{\ell \mid t_i\} \cdot \Pr\{p \mid t_i, \ell\} \cdot \Pr\{o \mid t_i\} \cdot \Pr\{a \mid f_j, t_i, p, o, \ell\} \quad (6)$$

Where $\Pr\{\ell \mid t_i\}$ is the probability of drawing a fragment of the inferred length, ℓ , given t_i , and is evaluated based on an observed empirical fragment length distribution. $\Pr\{p \mid t_i, \ell\}$ is the probability of the fragment starting at position p on t_i , computed using an empirical fragment start position distribution as defined in [14]. $\Pr\{o \mid t_i\}$ is the probability of obtaining a fragment aligning with the given orientation to t_i . This is determined by the concordance of the fragment with the user-specified library format. It is 1 if the alignment agrees with the library format and a user-defined prior value p_o otherwise. Finally, $\Pr\{a \mid f_j, t_i, p, o, \ell\}$ is the probability of generating alignment a of fragment f_j , given that it is drawn from t_i , with orientation o , and starting at position p and is of length ℓ ; this term is set to 1 when using quasi-mapping, and is given by equation (7) for traditional alignments. The parameters for all auxiliary models are learned during the streaming phase of the inference algorithm from the first N' observations (5,000,000 by default). These auxiliary terms can then be applied to all subsequent observations.

Sequence-specific bias It has been previously observed that the sequence surrounding the 5' and 3' ends of RNA-seq fragments has an effect on the likelihood that these fragments are selected for sequencing. If not accounted for, these biases can have a substantial effect on abundance estimates and can confound downstream analyses. To learn and correct for such biases, *Salmon* adopts a modification of the model introduced by Roberts et al. [4]. A (foreground) variable-length Markov model (VLMM) is trained on sequence windows surrounding the 5' ($b_{s+}^{5'}$) and 3' ($b_{s+}^{3'}$) read start positions. Then, a different (background) VLMM is trained on sequence windows drawn uniformly across known transcripts, each weighted by that transcript's abundance; the 5' and 3' background models are denoted as $b_{s-}^{5'}$ and $b_{s-}^{3'}$ respectively.

Fragment GC-bias In addition to the sequence surrounding the 5' and 3' ends of a fragment, it has also been observed that the GC-content of the entire fragment can play a substantial role in the likelihood that it will be selected for sequencing [5]. These biases are largely different than sequence-specific biases, and thus, accounting for both the context surrounding the fragments and the GC-content of the fragments themselves is important when one wishes to learn and correct for some of the most prevalent types of bias *in silico*. To account for fragment GC-bias, *Salmon* learns a foreground and background model of this fragment GC-bias (and defines the bias as the ratio of the score of a particular fragment under each). Our fragment GC-bias model consists of the observed distribution of sequenced fragments for every possible GC-content value (in practice, we discretize GC-content and maintain a distribution over 101 bins, for fragments with GC content ranging from 0 to 1 in increments of 0.01). The background model is trained on all possible fragments (drawn uniformly and according to the empirical fragment length distribution) across known transcripts, with each fragment weighted by that transcript's abundance. The foreground and background fragment GC-bias models are denoted as b_{gc+} and b_{gc-} respectively. Additionally, we note that sequence-specific and fragment GC biases do seem to display a conditional dependence. To account for this, *Salmon* learns 3 different bias models, each conditioned on the average GC content of the 5' and 3' sequence context of the fragment. A

separate model is trained and applied for fragments with average GC content between $[0, 0.33)$, $[0.33, 0.66)$, and $[0.66, 1]$.

Incorporating the bias models These bias models are used to re-estimate the effective length of each transcript, such that a transcript’s effective length now also takes into account the likelihood of sampling each possible fragment that transcript can produce — an approach to account for bias first introduced by Roberts et al. [4]. Before learning the bias-corrected effective lengths, the offline optimization algorithm is run for a small number of rounds (10 by default) to produce estimated abundances that are used when learning the background distributions for the various bias models. For a particular transcript t_i , the effective length becomes:

$$\tilde{\ell}'_i = \sum_{j=1}^{j \leq \ell_i} \sum_{k=1}^{k \leq f_i(j, L)} \frac{b_{gc+}(t_i, j, j+k)}{b_{gc-}(t_i, j, j+k)} \cdot \frac{b_{s+}^{5'}(t_i, j)}{b_{s-}^{5'}(t_i, j)} \cdot \frac{b_{s+}^{3'}(t_i, j+k)}{b_{s-}^{3'}(t_i, j+k)} \cdot \Pr\{X = j\}$$

where $\Pr\{X = j\}$ is the probability, under the empirical fragment length distribution, of observing a fragment of length j , L is the maximum observed fragment length, $f_i(j, L) = \min(\ell_i - j + 1, L)$, $b_{s+}^{5'}(t_i, j)$ is the score given to transcript t_i ’s j^{th} position under the foreground, 5' sequence-specific bias model ($b_{s-}^{5'}(t_i, j)$, $b_{s+}^{3'}(t_i, j)$, $b_{s-}^{3'}(t_i, j)$ are defined similarly) and $b_{gc+}(t_i, j, j+k)$ is the score given by the foreground fragment GC-content model for the subsequence of transcript t_i from position j to $j+k$ (and similarly for $b_{gc-}(t_i, j, j+k)$).

Once these bias-corrected lengths have been computed, they are used in all subsequent rounds of the offline inference phase (i.e. until the estimates of α — as defined in **Algorithms** — converge). Typically, the extra computational cost required to apply bias correction is rather small, and the learning and application of these bias weights is parallelized in *Salmon*. However, both the memory and time requirements of bias correction can be adjusted by the user to trade-off time and space with model fidelity. To make the computation of GC-fractions efficient for arbitrary fragments from the transcriptome, *Salmon* computes and stores the cumulative GC count for each transcript. To reduce memory consumption, this cumulative count can be sampled using the `--gcSizeSamp`. This will increase the time required to compute the GC-fraction for each

fragment by a constant factor. Similarly, when attempting to determine the effective length of a transcript, *Salmon* will evaluate the contribution of all fragments longer than the shortest 0.5% and shorter than the longest 0.5% of the full empirical fragment length distribution, that could derive from this transcript. The program option `--biasSpeedSamp` will instead sample fragment lengths at a user-defined factor, speeding up the computation of bias-corrected effective lengths by this factor, but coarsening the model in the process. All results reported in this manuscript where bias correction was included were run without either of these sampling options (i.e. using the full-fidelity model).

Alignment model

When *Salmon* is given read alignments as input, it can learn and apply a model of read alignments to help assess the probability that a fragment originated from a particular locus. Specifically, *Salmon*'s alignment model is a spatially varying first-order Markov model over the set of CIGAR symbols and nucleotides. To account for the fact that substitution and indel rates can vary spatially over the length of a read, we partition each read into a fixed number of bins (4 by default) and learn a separate model for each of these bins. This allows us to learn spatially varying effects without making the model itself too large (as if, for example, we had attempted to learn a separate model for each position in the read). Given the CIGAR string $s = s_0, \dots, s_{|s|}$ for an alignment a , we compute the probability of a as:

$$\Pr \{a \mid f_j, t_i, p, o, \ell\} = \Pr \{s_0\} \prod_{k=1}^{|s|} \Pr_{(\mathcal{M}_k)} \{s_{k-1} \rightarrow s_k \mid f_j, t_i, p, o, \ell\} \quad (7)$$

where $\Pr \{s_0\}$ is the start probability and $\Pr_{(\mathcal{M}_k)} \{\cdot\}$ is the transition probability under the model at the k^{th} position of the read (i.e., in the bin corresponding to position k). To compute these probabilities, *Salmon* parses the CIGAR string s and moves appropriately along both the fragment f_j and the reference transcript t_i , and computes the probability of transitioning to the next observed state in the alignment (a tuple consisting of the CIGAR operation, and the nucleotides in

the fragment and reference) given the current state of the model. The parameters of this Markov model are learned from sampled alignments in the online phase of the algorithm (see **Algorithm 1**). When quasi-mapping is used instead of user-provided alignments, the probability of the “alignment” is not taken into account (i.e. $\Pr \{a \mid f_j, t_i, p, o, \ell\}$ is set to 1 for each mapping).

Algorithms

Salmon consists of three components: a lightweight-mapping model, an online phase that estimates initial expression levels and model parameters and constructs equivalence classes over the input fragments, and an offline phase that refines these expression estimates. The online and offline phases together optimize the estimates of α which is a vector of weighted estimates of read counts. Each method can compute η directly from these parameters.

The online phase uses a variant of stochastic, collapsed variational Bayesian inference [22]. The offline phase applies either a standard EM algorithm, or a variational Bayesian EM algorithm [21] over a reduced representation of the data represented by the equivalence classes until a data-dependent convergence criterion is satisfied. An overview of our method is given in **Supplementary Fig. 1**, and we describe each component in more detail below.

Online phase

The online phase of *Salmon* attempts to solve the variational Bayesian inference problem described in **Objectives and models for abundance estimation**, and optimizes a collapsed variational objective function [19] using a variant of stochastic collapsed Variational Bayesian inference [22]. The inference procedure is a streaming algorithm, similar to [15], but it updates estimated read counts α after every small group B^τ (called a mini-batch) of observations, and processing of mini-batches is done asynchronously and in parallel. The pseudo-code for the algorithm is given in **Algorithm 1**.

Algorithm 1 Laissez-faire SCVB0

```

1: while  $B^\tau \leftarrow \text{pop}(\text{work-queue})$  do
2:    $\hat{x} \leftarrow 0$ 
3:   for read  $r \in B^\tau$  do
4:      $x \leftarrow 0$ 
5:     for alignment  $a$  of  $r$  do
6:        $y \leftarrow$  the transcript involved in alignment  $a$ 
7:        $x_y \leftarrow x_y + \alpha_y \cdot \Pr\{a \mid y\}$   $\triangleright$  Add  $a$ 's contribution to the local weight for transcript
         $y$ 
8:     end for  $\triangleright$  Normalize the contributions for all alignments of  $r$ 
9:     for alignment  $a$  of  $r$  do
10:       $y \leftarrow$  the transcript involved in alignment  $a$ 
11:       $\hat{x}_y \leftarrow \hat{x}_y + \frac{x_y}{\sum_{y' \in r} x_{y'}}$ 
12:    end for
13:    Sample  $a \in r$  and update auxiliary models using  $a$ 
14:  end for
15:   $\alpha \leftarrow \alpha + v^\tau \cdot \hat{x}$   $\triangleright$  Update the global weights with local observations from  $B^\tau$ 
16: end while

```

The observation weight for mini-batch B^τ , v^τ , in line 15 of **Algorithm 1** is an increasing sequence in τ , and is set, as in [15], to adhere to the Robbins-Monroe conditions. Here, the α represent the (weighted) estimated counts of fragments originating from each transcript. Using this method, the expected value of η can be computed directly from α using equation (16). We employ a *weak* Dirichlet conjugate-prior with $\alpha_i^0 = 0.001 \cdot \tilde{\ell}_i$ for all $t_i \in \mathcal{T}$. As outlined in [22], the SCVB0 inference algorithm is similar to variants of the online-EM [23] algorithm with a modified prior. The procedure in **Algorithm 1** is run independently by as many worker threads as the user has specified. The threads share a single work-queue upon which a parsing thread places mini-batches of alignment groups. An alignment group is simply the collection of all alignments (i.e. all multi-mapping locations) for a particular read. The mini-batch itself consists of a collection of some small, fixed number of alignment groups (1,000 by default). Each worker thread processes one alignment group at a time, using the current weights of each transcript and the current auxiliary parameters to estimate the probability that a read came from each potential transcript of origin. The processing of mini-batches occurs in parallel, so that very little synchronization is required, only an atomic compare-and-swap loop to update the global

transcript weights at the end of processing of each mini-batch — hence the moniker *laissez-faire* in the label of **Algorithm 1**. This lack of synchronization means that when estimating x_y , we cannot be certain that the most up-to-date values of α are being used. However, due to the stochastic and additive nature of the updates, this has little-to-no detrimental effect [24]. The inference procedure itself is generic over the type of alignments being processed; they may be either regular alignments (e.g. coming from a `bam` file), or quasi-mappings computed from the raw reads (e.g. coming from `FASTA/Q` files). After the entire mini-batch has been processed, the global weights for each transcript α are updated. These updates are *sparse*; i.e. only transcripts that appeared in some alignment in mini-batch B^τ will have their global weight updated after B^τ has been processed. This ensures, as in [15], that updates to the parameters α can be performed efficiently.

Equivalence classes

During its online phase, in addition to performing streaming inference of transcript abundances, *Salmon* also constructs a highly-reduced representation of the sequencing experiment. Specifically, *Salmon* constructs “rich” equivalence classes over all of the sequenced fragments. Collapsing fragments into equivalence classes is a well-established idea in the transcript quantification literature, and numerous different notions of equivalence classes have been previously introduced, and shown to greatly reduce the time required to perform iterative optimization such as that described in **Offline phase**. For example, Salzman et al. [25] first introduced the notion of factorizing the likelihood function to speed up inference by collapsing fragments that align to the same exons or exon junctions (as determined by a provided annotation) into equivalence classes. Similarly, Nicolae et al. [26] used equivalence classes over fragments to reduce memory usage and speed up inference — they define as equivalent any pair of fragments that align to the same set of transcripts and whose compatibility weights (i.e. conditional probabilities) with respect to those transcripts are proportional. Patro et al. [9] define equivalence classes over k-mers, treating as equivalent any k-mers that appear in the same set of transcripts at

the same frequency, and use this factorization of the likelihood function to speed up optimization. Bray et al. [10] define equivalence classes over fragments, and define as equivalent any fragments that pseudoalign to the same set of transcripts — this is similar to the notion adopted by Nicolae et al., except that no restriction is placed on the proportionality of compatibility weights (since these are not computed).

To compute equivalence classes, we define an equivalence relation \sim over fragments. Let $A(\mathcal{T}, f_x)$ denote the set of quasi-mappings (or alignments) of f_x to the transcriptome \mathcal{T} , and let $M(f_x) = \{t_i \mid (t_i, p_i, o_i) \in A(\mathcal{T}, f_x)\}$ be the set of transcripts to which f_x maps according to $A(\mathcal{T}, f_x)$. We say $f_x \sim f_y$ if and only if $M(f_x) = M(f_y)$. Fragments which are equivalent are grouped together for the purpose of inference. *Salmon* builds up a set of fragment-level equivalence classes by maintaining an efficient concurrent cuckoo hash map [27]. To construct this map, we associate each fragment f_x with $t^x = M(f_x)$, which we will call the label of the fragment. Then, we query the hash map for t^x . If this key is not in the map, we create a new equivalence class with this label, and set its count to 1. Otherwise, we increment the count of the equivalence class that we find in the map with this label. The efficient, concurrent nature of the data structure means that many threads can simultaneously query and write to the map while encountering very little contention. Each key in the hash map is associated with a value that we call a “rich” equivalence class. For each equivalence class \mathcal{C}^j , we retain a count $d^j = |\mathcal{C}^j|$, which is the total number of fragments contained within this class. We also maintain, for each class, a weight vector w^j . The entries of this vector are in one-to-one correspondence with transcripts i in the label of this equivalence class such that

$$w_i^j = \frac{\sum_{f \in \mathcal{C}^j} \Pr\{f \mid t_i\}}{\sum_{t_k \in t^j} \sum_{f \in \mathcal{C}^j} \Pr\{f \mid t_k\}}. \quad (8)$$

That is, w_i^j is the average conditional probability of observing a fragment from \mathcal{C}^j given t_i over all fragments in this equivalence class. Though the likelihood function over equivalence classes that considers these weights (Equation (10)) is no longer exactly equivalent to the likelihood defined

over all fragments (Equation (9)), these weights nonetheless allow us to take into consideration the conditional probabilities specified in the full model, without having to continuously reconsider each of the fragments in \mathcal{F} . There is a spectrum of possible representations of “rich” equivalence classes. This spectrum spans from notion adopted here, which collapses all conditional probabilities into a single aggregate scalar, to an approach that clusters together fragments based not only on the transcripts to which they match, but on the vector of normalized conditional probabilities for each of these transcripts. The former approach represents a more coarse-grained approximate factorization of the likelihood function while the latter represents a more fine-grained approximation. We believe that studying how these different notions of equivalence classes affect the factorization of the likelihood function, and hence its optimization, is an interesting direction for future work.

Offline phase

In its offline phase, which follows the online phase, *Salmon* uses the “rich” equivalence classes learned during the online phase to refine the inference. Given the set \mathcal{C} of rich equivalence classes of fragments, we can use an expectation maximization (EM) algorithm to optimize the likelihood of the parameters given the data. The abundances η can be computed directly from α , and we compute maximum likelihood estimates of these parameters which represent the estimated counts (i.e. number of fragments) deriving from each transcript, where:

$$\mathcal{L} \{ \alpha \mid \mathcal{F}, \mathbf{Z}, \mathcal{T} \} = \prod_{j=1}^N \sum_{i=1}^M \hat{\eta}_i \Pr \{ f_j \mid t_i \} \quad (9)$$

and $\hat{\eta}_i = \frac{\alpha_i}{\sum_j \alpha_j}$. If we write this same likelihood in terms of the equivalence classes \mathcal{C} , we have:

$$\mathcal{L} \{ \alpha \mid \mathcal{F}, \mathbf{Z}, \mathcal{T} \} \approx \prod_{\mathcal{C}^j \in \mathcal{C}} \left(\sum_{t_i \in \mathcal{C}^j} \hat{\eta}_i w_i^j \right)^{d^j} . \quad (10)$$

EM update rule This likelihood, and hence that represented in equation (9), can then be optimized by applying the following update equation iteratively

$$\alpha_i^{u+1} = \sum_{c^j \in \mathcal{C}} d^j \left(\frac{\alpha_i^u w_i^j}{\sum_{t_k \in t^j} \alpha_k^u w_k^j} \right). \quad (11)$$

We apply this update equation until the maximum relative difference in the α parameters satisfies:

$$\Delta(\alpha^u, \alpha^{u+1}) = \max_i \frac{|\alpha_i^u - \alpha_i^{u+1}|}{\alpha_i^{u+1}} < 1 \times 10^{-2} \quad (12)$$

for all $\alpha_i^{u+1} > 1 \times 10^{-8}$. Let α' be the estimates after having achieved convergence. We can then estimate η_i by $\hat{\eta}_i$, where:

$$\hat{\eta}_i = \frac{\alpha'_i}{\sum_j \alpha'_j}. \quad (13)$$

Variational Bayes optimization Instead of the standard EM updates of equation (11), we can, optionally, perform Variational Bayesian optimization by applying VBEM updates as in [20], but adapted to be with respect to the equivalence classes:

$$\alpha_i^{u+1} = \sum_{c^j \in \mathcal{C}} d^j \left(\frac{e^{\gamma_i^u} w_i^j}{\sum_{t_k \in t^j} e^{\gamma_k^u} w_k^j} \right), \quad (14)$$

where:

$$\gamma_i^u = \Psi(\alpha_i^0 + \alpha_i^u) - \Psi\left(\sum_k \alpha_k^0 + \alpha_k^u\right). \quad (15)$$

Here, $\Psi(\cdot)$ is the digamma function, and, upon convergence of the parameters, we can obtain an estimate of the expected value of the posterior nucleotide fractions as:

$$\mathbb{E}\{\eta_i\} = \frac{\alpha_i^0 + \alpha'_i}{\sum_j \alpha_j^0 + \alpha'_j} = \frac{\alpha_i^0 + \alpha'_i}{\hat{\alpha}^0 + N}, \quad (16)$$

where $\hat{\alpha}^0 = \sum_{i=1}^M \alpha_i^0$. Variational Bayesian optimization in the offline-phase of *Salmon* is selected by passing the `--useVBOpt` flag to the *Salmon* `quant` command.

Sampling from the posterior

After the convergence of the parameter estimates has been achieved in the offline phase, it is possible to draw samples from the posterior distribution using collapsed, blockwise Gibbs sampling over the equivalence classes. Samples can be drawn by iterating over the equivalence classes, and re-sampling assignments for some fraction of fragments in each class according to the multinomial distribution defined by holding the assignments for all other fragments fixed. Many samples can be drawn quickly, since many Gibbs chains can be run in parallel. Further, due to the accuracy of the preceding inference, the chains begin sampling from a relatively high probability position in the latent variable space almost immediately. These posterior samples can be used to obtain estimates for quantities of interest about the posterior distribution, such as its variance, or to produce credible intervals. When *Salmon* is passed the `--numGibbsSamples` option, it will draw a number of posterior samples that is provided to this option.

Additionally, inspired by *kallisto* [10], *Salmon* also provides the ability to draw bootstrap samples, which is an alternative way to assign confidence to the estimates returned by the main inference algorithm. Bootstrap samples can be drawn by passing the `--numBootstraps` option to *Salmon* with the argument determining the number of bootstraps to perform. The bootstrap sampling process works by sampling (with replacement) counts for each equivalence class, and then re-running the offline inference procedure (either the EM or VBEM algorithm) for each bootstrap sample.

Validation

Metrics for accuracy

Throughout this paper, we use several different different metrics to summarize the agreement of the estimated TPM for each transcript with the TPM computed from simulated counts. While most of these metrics are commonly used and self-explanatory, we here describe the computation of the mean absolute relative difference (MARD), which is, less common than some of the other

metrics.

The MARD is computed using the absolute relative difference ARD_i for each transcript i :

$$ARD_i = \begin{cases} 0 & \text{if } x_i = y_i = 0 \\ \frac{|x_i - y_i|}{x_i + y_i} & \text{otherwise} \end{cases}, \quad (17)$$

where x_i is the true value of the TPM, and y_i is the estimated TPM. The relative difference is bounded above by 1, and takes on a value of 0 whenever the prediction perfectly matches the truth. To compute the mean absolute relative difference, we simply take $MARD = \frac{1}{M} \sum_{i=1}^M ARD_i$. We note that *Salmon* and *kallisto*, by default, truncate very tiny expression values to 0. For example, any transcript estimated to produce $< 1 \times 10^{-8}$ reads is assigned an estimated read count of 0 (which, likewise, affects the TPM estimates). However, *eXpress* does not perform such a truncation, and very small, non-zero values may have a negative effect on the MARD metric. To mitigate such effects, we first truncate to 0 all TPMs less than 0.01 before computing the MARDs.

Ground truth simulated data

To assess accuracy in a situation where the true expression levels are known, we generate synthetic data sets using both *Polyester* [13] and *RSEM-sim* [14].

***RSEM-sim* simulations** To generate data with *RSEM-sim*, we follow the procedure used in [10]. *RSEM* was run on sample NA12716_7 from the GEUVADIS RNA-seq data to learn model parameters and estimate true expression, and the learned model was then used to generate 20 different simulated datasets, each consisting of 30 million 75 bp paired-end reads.

***Polyester* simulations** In addition to the ability to generate reads, *Polyester* allows simulating experiments with differential transcript expression and biological variability. Thus, we can assess not only the accuracy of the resulting estimates, but also how these estimates would perform in a typical downstream analysis task like differential expression testing.

The *Polyester* simulation of an RNA-seq experiment with empirically-derived fragment GC bias was created as follows: The transcript abundance quantifications from *RSEM* run on NA12716_7 of the GEUVADIS RNA-seq data [11] were summed to the gene-level using version 75 of the Ensembl gene annotation for GRCh37. Subsequently, whole-transcriptome simulation was carried out using *Polyester*. Abundance (TPMs) was allocated to isoforms within a gene randomly using the following rule: for genes with two isoforms, TPMs were either (i) split according to a flat Dirichlet distribution ($\alpha = (1, 1)$) or (ii) attributed to a single isoform. The choice of (i) vs (ii) was decided by a Bernoulli trial with probability 0.5. For genes with three or more isoforms, TPMs were either (i) split among three randomly chosen isoforms according to a flat Dirichlet distribution ($\alpha = (1, 1, 1)$) or (ii) attributed to a single isoform. Again, (i) vs (ii) was decided by a Bernoulli trial with probability 0.5. The choice of distributing expression among three isoforms was motivated by exploratory data analysis of estimated transcript abundance revealing that for most genes nearly all of expression was concentrated in the first three isoforms for genes with four or more isoforms.

Expected counts for each transcript were then generated according to the transcript-level TPMs, multiplied by the transcript lengths. 40 million 100bp paired-end reads were simulated using the *Polyester* software for each of 16 samples, and 10% of transcripts were chosen to be differentially expressed across an 8 vs 8 sample split. The fold change was chosen to be either $\frac{1}{2}$ or 2 with probability of 0.5. Fragments were down-sampled with Bernoulli trials according to an empirically-derived fragment GC content dependence estimated with *alpine* [5] on RNA-seq samples from the GEUVADIS project. The first 8 GEUVADIS samples exhibited weak GC content dependence while the last 8 samples exhibited more severe fragment-level GC bias. Paired-end fragments were then shuffled before being supplied to transcript abundance quantifiers. Estimated expression was compared to true expression calculated on transcript counts (before these counts were down-sampled according to the empirically-derived fragment GC bias curve), divided by effective transcript length and scaled to TPM. Global differences across condition for all methods were removed using a scaling factor per condition. Differences across

condition for the different methods' quantifications were tested using a t-test of $\log_2(\text{TPM} + 1)$.

Software versions and options

All tests were performed with *eXpress* v1.5.1, *kallisto* v0.43.0, *Salmon* v0.7.1 and Bowtie2 v2.2.4. Reads were aligned with Bowtie2 using the parameters `--no-discordant -k 200`, and `-p` to set the number of threads. On the *RSEM-sim* data, all methods were run *without* bias correction. On all other datasets, methods were run with bias correction unless otherwise noted. Additionally, on the *Polyester* simulated data, *Salmon* was run with the option `--noBiasLengthThreshold`, which allows bias correction, even for very short transcripts, since we were most interested in assessing the maximum sensitivity of the model.

GEUVADIS data

The analyses presented in **Fig. 1d**, **Supplementary Table 1** and **Supplementary Fig. 5** were carried out on a subset of 30 samples from the publicly-available GEUVADIS [11] data. The accessions used and the information about the center at which the libraries were prepared and sequenced is recorded in **Supplementary Table 2**. All methods were run with bias correction enabled, using a transcriptome built with the RefSeq gene annotation file and the genome FASTA contained within the hg19 Illumina iGenome, in order to allow for comparison with the results in [5]. For each transcript, a t-test was performed, comparing $\log_2(\text{TPM}+1)$ from 15 samples from one sequencing center against 15 samples from another sequencing center. Because the samples are from the same human population, it is expected that there would be few to no true differences in transcript abundance produced by this comparison. *P* values were then adjusted using the method of Benjamini-Hochberg, over the transcripts with mean TPM > 0.1. The number of positives for given false discovery rates was then reported for each method, by taking the number of transcripts with adjusted *p* value less than a given threshold.

SEQC data

The consistency analysis presented in **Supplementary Fig. 2** was carried out on a subset of the publicly-available SEQC [28] data. Specifically, the accessions used, along with the corresponding information about the center at which they were sequences is recorded in **Supplementary Table 3**. For each sample, “same center” comparisons were made between all unique pairs of replicates labeled as coming from the same sequencing center, while “different center” comparisons were made between all unique pairs of replicates labeled as coming from different centers (“Center” column of **Supplementary Table 3**).

References for Online Methods

- [19] James Hensman, Panagiotis Papastamoulis, Peter Glaus, Antti Honkela, and Magnus Rattray. Fast and accurate approximate inference of transcript expression from RNA-seq data. *Bioinformatics*, 31(24):3881–3889, 2015.
- [20] Naoki Nariai, Kaname Kojima, Takahiro Mimori, Yukuto Sato, Yosuke Kawai, Yumi Yamaguchi-Kabata, and Masao Nagasaki. TIGAR2: sensitive and accurate estimation of transcript isoform expression with longer RNA-Seq readsonline. *BMC Genomics*, 15(Suppl 10):S5, 2014.
- [21] Christopher M Bishop et al. *Pattern Recognition and Machine Learning*, volume 4. Springer, New York, 2006.
- [22] James Foulds, Levi Boyles, Christopher DuBois, Padhraic Smyth, and Max Welling. Stochastic collapsed variational Bayesian inference for latent Dirichlet allocation. In *Proceedings of the 19th ACM SIGKDD International Conference on Knowledge Discovery and Data Mining*, pages 446–454. ACM, 2013.
- [23] Olivier Cappé. Online expectation-maximisation. *Mixtures: Estimation and Applications*, pages 1–53, 2011.

- [24] Cho-Jui Hsieh, Hsiang-Fu Yu, and Inderjit S Dhillon. PASSCoDe: Parallel ASynchronous Stochastic dual Co-ordinate Descent. *arXiv preprint arXiv:1504.01365*, 2015.
- [25] Julia Salzman, Hui Jiang, and Wing Hung Wong. Statistical modeling of RNA-Seq data. *Statistical science: a review journal of the Institute of Mathematical Statistics*, 26(1), 2011.
- [26] Marius Nicolae, Serghei Mangul, Ion I Mandoiu, and Alex Zelikovsky. Estimation of alternative splicing isoform frequencies from RNA-Seq data. *Algorithms for Molecular Biology*, 6(1):9, 2011.
- [27] Xiaozhou Li, David G Andersen, Michael Kaminsky, and Michael J Freedman. Algorithmic improvements for fast concurrent cuckoo hashing. In *Proceedings of the Ninth European Conference on Computer Systems*, page 27. ACM, 2014.
- [28] SEQC/MAQC-III Consortium et al. A comprehensive assessment of RNA-seq accuracy, reproducibility and information content by the Sequencing Quality Control Consortium. *Nature Biotechnology*, 32(9):903–914, 2014.

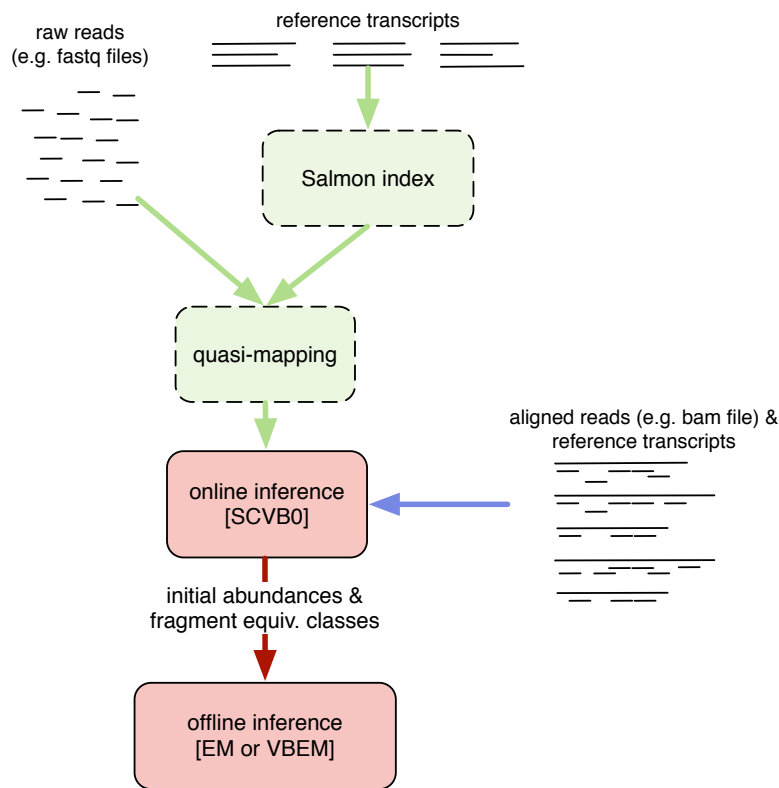
Supplementary Material

for

“*Salmon* provides accurate, fast, and bias-aware transcript expression estimates using dual-phase inference”

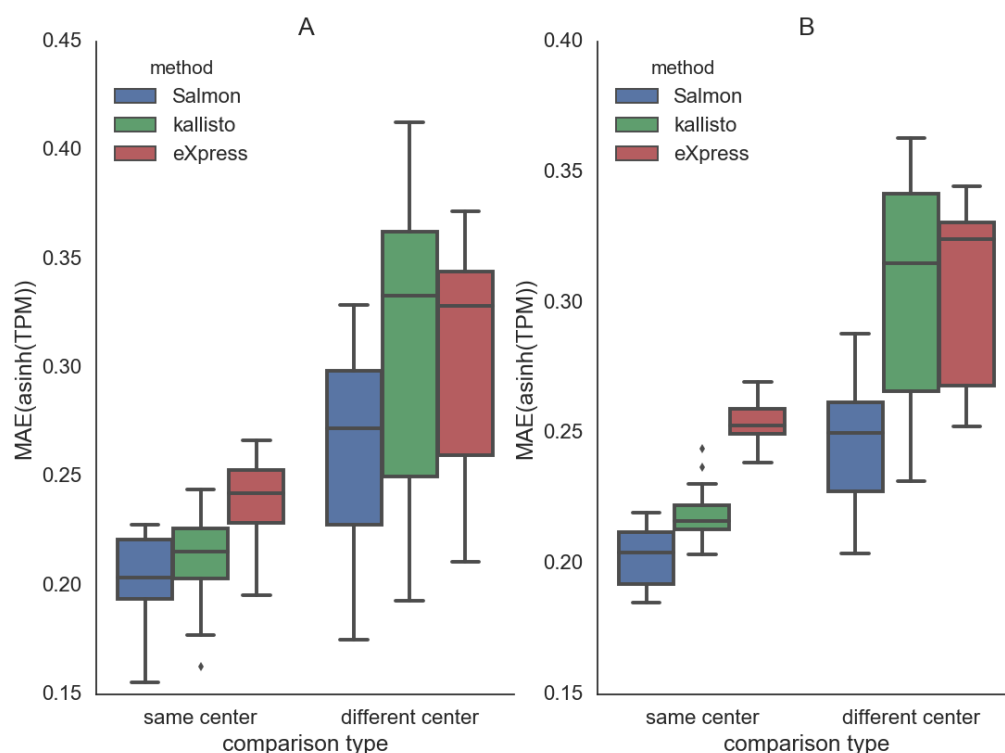
by Rob Patro, Geet Duggal, Michael I. Love, Rafael A. Irizarry and Carl Kingsford

Supplementary Figure 1: Overview of Salmon's method and components.



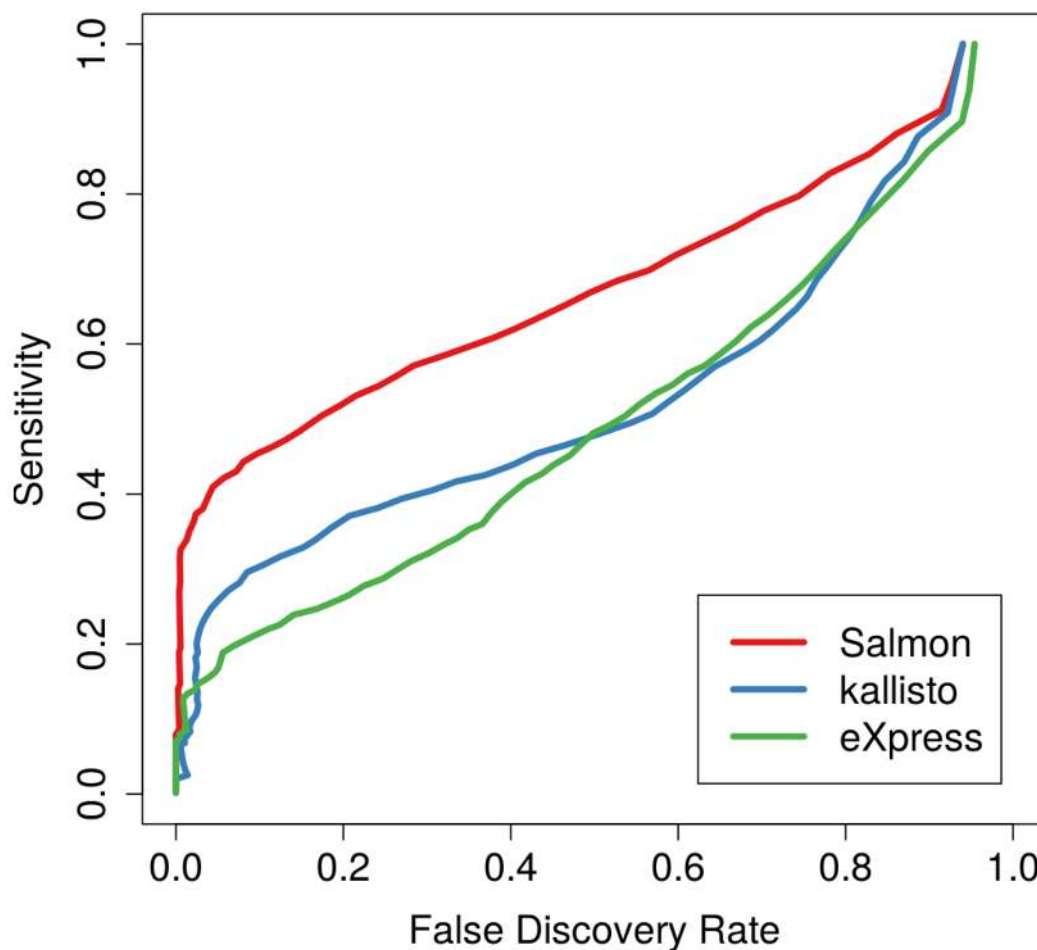
Supplementary Figure 1: Overview of *Salmon*'s method and components. *Salmon* accepts either raw (green arrows) or aligned reads (blue arrow) as input, performs an online inference when processing fragments or alignments, builds equivalence classes over these fragments and subsequently refines abundance estimates using an offline inference algorithm on a reduced representation of the data.

Supplementary Figure 2: Consistency of estimates on SEQC data within and between centers



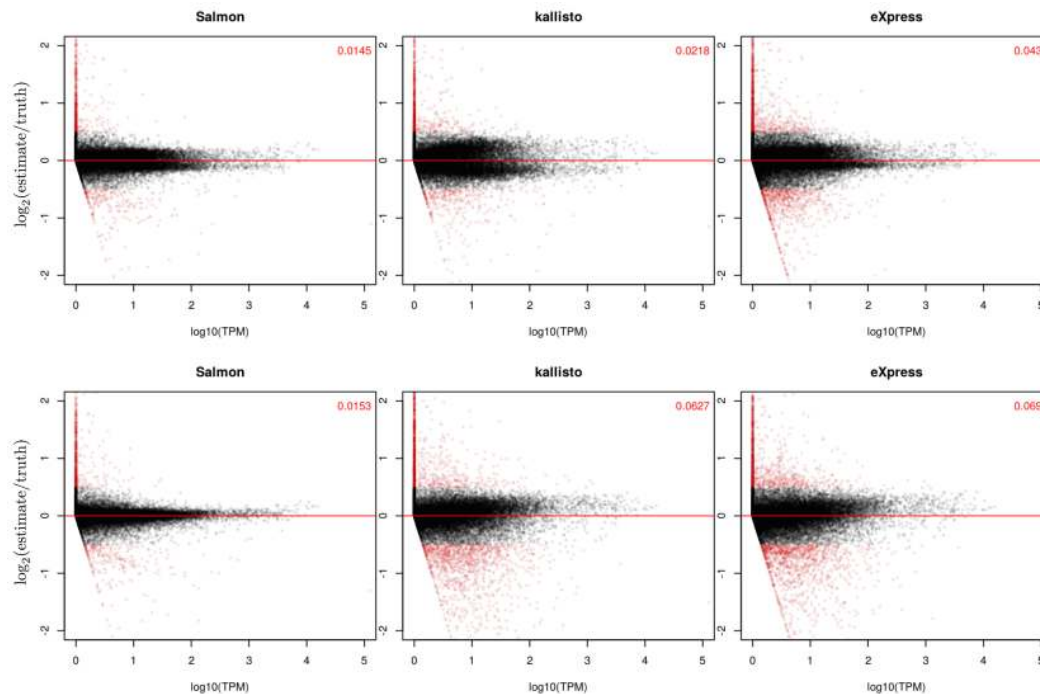
Supplementary Figure 2: The distribution of the mean absolute error of (inverse hyperbolic sine-transformed) TPMs between different replicates of data from the SEQC [28] study. The A sample corresponds to universal human reference tissue (UHRR) and the B sample corresponds to human brain tissue (HBRR). When comparing the replicates that were sequenced at different centers, the inter-replicate distances are larger. However, we observe that *Salmon*'s bias correction methodology results in improved consistency (i.e. reduced distance) compared to the estimates produced by other methods, especially when comparing replicates sequenced at different centers, where we expect the effects of bias to be more pronounced.

Supplementary Figure 3: FDR vs. sensitivity on *Polyester* simulated data.



Supplementary Figure 3: The false discovery rate (FDR) vs. the sensitivity of *Salmon*, *kallisto* and *eXpress* on *Polyester* simulated RNA-seq data using empirically-derived fragment GC bias profiles. All methods were run with bias-correction enabled, but only *Salmon*'s model incorporates corrections for fragment GC bias. This leads to a large improvement in sensitivity at almost every FDR value.

Supplementary Figure 4: Abundance vs. fold change accuracy on *Polyester* simulated data.



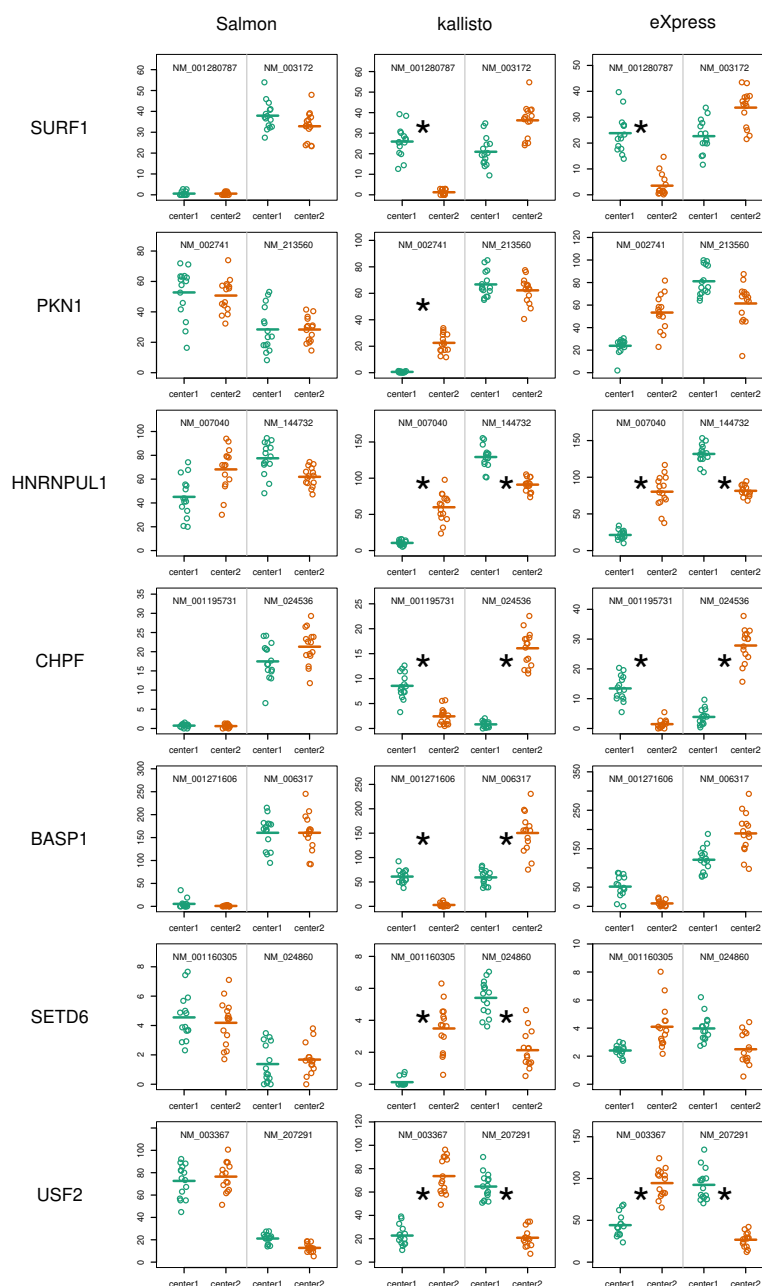
Supplementary Figure 4: The log₂ fold change between the estimated and true abundances as a function of the true abundance (measured in TPM), for all 3 methods and for all replicates of both simulated “conditions” (each row displays points from all samples within a given condition). The top row corresponds to the 8 samples simulated from the data showing the weak fragment GC content bias, while the bottom row corresponds to the 8 samples simulated from the data showing the stronger fragment GC content bias. Points with an estimated log₂ fold change of > 0.5 or < -0.5 are colored red. The fraction of red points appears in the upper right-hand corner of each plot. *Salmon* consistently demonstrates log fold changes closer to 0 than either *kallisto* or *eXpress*, across most of the range of expression.

Supplementary Table 1: Gene Level GEUVADIS DE

Supplementary Table 1: The number of genes identified as differentially expressed at a target FDR of 1% for two groups of GEUVADIS samples. The contrast between samples is a technical confound, and we expect little-to-no true DE. Gene-level TPM was computed by summing the TPM of the isoforms, and differential testing was performed as described in Methods.

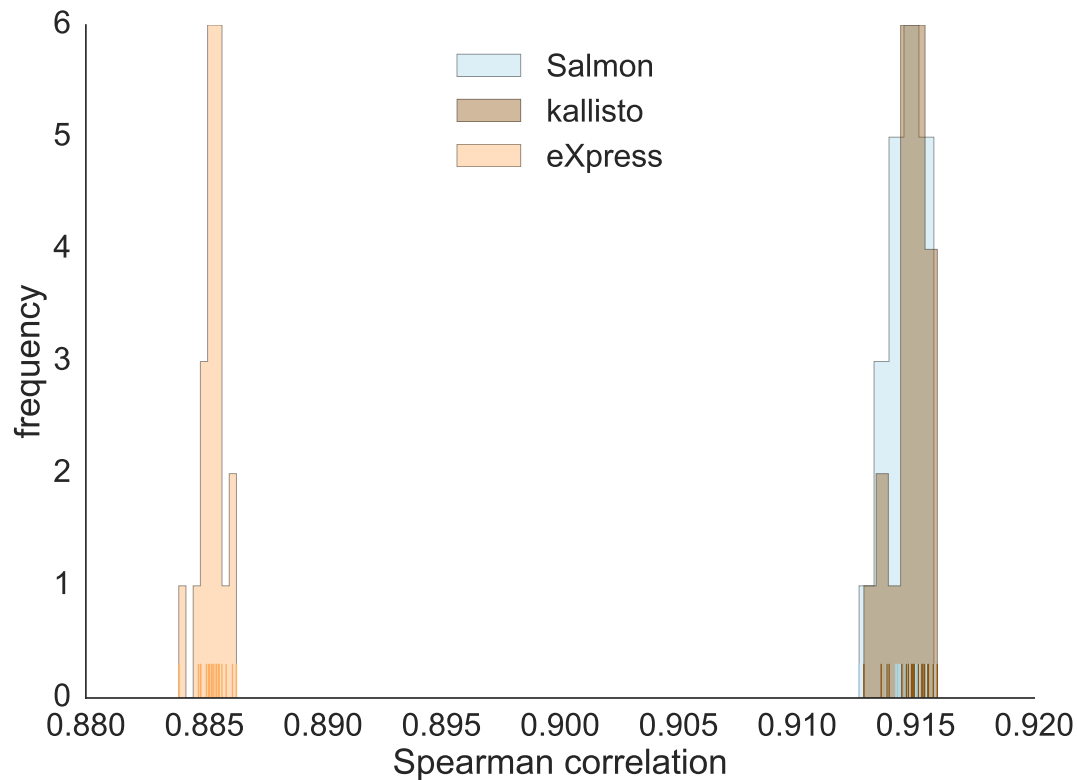
<i>Salmon</i>	<i>kallisto</i>	<i>eXpress</i>
455	1200	1582

Supplementary Figure 5: *Salmon* reduces false isoform switching



Supplementary Figure 5: Transcripts demonstrating dominant isoform switching that results from technical bias. In the quantification estimates computed using *kallisto* and *eXpress*, these two-isoform genes show a change in the dominant isoform between conditions (an asterisk denotes a t-test on $\log_2(\text{TPM}+1)$ with $p < 1 \times 10^{-6}$). However, *Salmon* directly corrects for technical biases that appear to underlay differences across sequencing center, revealing that the dominant isoform has not, in fact, switched across center.

Supplementary Figure 6: Quantification accuracy for *Salmon*, *kallisto* and *eXpress* using *RSEM-sim* data.



Supplementary Figure 6: This plot shows the distribution of Spearman correlations over all 20 replicates of the *RSEM-sim* data for *Salmon*, *kallisto* and *eXpress*. *Salmon* and *kallisto* yield very similar distributions of correlations (no statistically significant difference), while both methods yield correlations greater than that of *eXpress* (Mann-Whitney *U* test, $p = 3.39780 \times 10^{-8}$).

Supplementary Table 2: GEUVADIS samples used for specificity assessment.

Population	Center	Assay	Sample	Experiment	Run accession
TSI	UNIGE	NA20503.1.M_111124_5	ERS185497	ERX163094	ERR188297
TSI	UNIGE	NA20504.1.M_111124_7	ERS185242	ERX162972	ERR188088
TSI	UNIGE	NA20505.1.M_111124_6	ERS185048	ERX163009	ERR188329
TSI	UNIGE	NA20507.1.M_111124_7	ERS185412	ERX163158	ERR188288
TSI	UNIGE	NA20508.1.M_111124_2	ERS185362	ERX163159	ERR188021
TSI	UNIGE	NA20514.1.M_111124_4	ERS185217	ERX163062	ERR188356
TSI	UNIGE	NA20519.1.M_111124_5	ERS185167	ERX162948	ERR188145
TSI	UNIGE	NA20525.1.M_111124_1	ERS185212	ERX163022	ERR188347
TSI	UNIGE	NA20536.1.M_111124_1	ERS185156	ERX163042	ERR188382
TSI	UNIGE	NA20540.1.M_111124_2	ERS185349	ERX162940	ERR188436
TSI	UNIGE	NA20541.1.M_111124_4	ERS185125	ERX163043	ERR188052
TSI	UNIGE	NA20581.1.M_111124_4	ERS185181	ERX162937	ERR188402
TSI	UNIGE	NA20589.1.M_111124_3	ERS185057	ERX162793	ERR188343
TSI	UNIGE	NA20757.1.M_111124_1	ERS185169	ERX162732	ERR188295
TSI	UNIGE	NA20761.1.M_111124_7	ERS185420	ERX163049	ERR188479
TSI	CNAG_CRG	NA20524.2.M_111215_8	ERS185498	ERX162769	ERR188204
TSI	CNAG_CRG	NA20527.2.M_111215_7	ERS185082	ERX163033	ERR188317
TSI	CNAG_CRG	NA20529.2.M_111215_6	ERS185422	ERX162984	ERR188453
TSI	CNAG_CRG	NA20530.2.M_111215_6	ERS185442	ERX163025	ERR188258
TSI	CNAG_CRG	NA20534.2.M_111215_8	ERS185144	ERX162843	ERR188114
TSI	CNAG_CRG	NA20543.2.M_111215_5	ERS185134	ERX163170	ERR188334
TSI	CNAG_CRG	NA20586.2.M_111215_7	ERS185426	ERX162880	ERR188353
TSI	CNAG_CRG	NA20758.2.M_111215_8	ERS185342	ERX162819	ERR188276
TSI	CNAG_CRG	NA20765.2.M_111215_5	ERS185306	ERX162794	ERR188153
TSI	CNAG_CRG	NA20771.2.M_111215_7	ERS185108	ERX163165	ERR188345
TSI	CNAG_CRG	NA20786.2.M_111215_8	ERS185069	ERX162761	ERR188192
TSI	CNAG_CRG	NA20790.2.M_111215_6	ERS185378	ERX163152	ERR188155
TSI	CNAG_CRG	NA20797.2.M_111215_6	ERS185263	ERX162729	ERR188132
TSI	CNAG_CRG	NA20810.2.M_111215_7	ERS185427	ERX162968	ERR188408
TSI	CNAG_CRG	NA20814.2.M_111215_6	ERS185127	ERX163109	ERR188265

Supplementary Table 2: Accession information for GEUVADIS samples.

Supplementary Table 3: SEQC samples used for consistency assessment.

Run accession	Replicate	Sample	Center	Run accession	Replicate	Sample	Center
SRR896664	1	A	BGI	SRR897077	3	A	CNL
SRR896663	1	A	BGI	SRR897078	3	A	CNL
SRR896665	1	A	BGI	SRR897079	3	A	CNL
SRR896666	1	A	BGI	SRR897080	3	A	CNL
SRR896667	1	A	BGI	SRR897081	3	A	CNL
SRR896668	1	A	BGI	SRR897082	3	A	CNL
SRR896679	2	A	BGI	SRR897092	4	A	CNL
SRR896680	2	A	BGI	SRR897093	4	A	CNL
SRR896681	2	A	BGI	SRR897094	4	A	CNL
SRR896682	2	A	BGI	SRR897095	4	A	CNL
SRR896683	2	A	BGI	SRR897096	4	A	CNL
SRR896684	2	A	BGI	SRR897097	4	A	CNL
SRR896695	3	A	BGI	SRR897407	1	A	MAY
SRR896696	3	A	BGI	SRR897408	1	A	MAY
SRR896697	3	A	BGI	SRR897409	1	A	MAY
SRR896698	3	A	BGI	SRR897410	1	A	MAY
SRR896699	3	A	BGI	SRR897411	1	A	MAY
SRR896700	3	A	BGI	SRR897412	1	A	MAY
SRR896711	4	A	BGI	SRR897423	2	A	MAY
SRR896712	4	A	BGI	SRR897424	2	A	MAY
SRR896713	4	A	BGI	SRR897425	2	A	MAY
SRR896714	4	A	BGI	SRR897426	2	A	MAY
SRR896715	4	A	BGI	SRR897427	2	A	MAY
SRR896716	4	A	BGI	SRR897428	2	A	MAY
SRR897047	1	A	CNL	SRR897439	3	A	MAY
SRR897048	1	A	CNL	SRR897440	3	A	MAY
SRR897049	1	A	CNL	SRR897441	3	A	MAY
SRR897050	1	A	CNL	SRR897442	3	A	MAY
SRR897051	1	A	CNL	SRR897443	3	A	MAY
SRR897052	1	A	CNL	SRR897444	3	A	MAY
SRR897062	2	A	CNL	SRR897455	4	A	MAY
SRR897063	2	A	CNL	SRR897456	4	A	MAY
SRR897064	2	A	CNL	SRR897457	4	A	MAY
SRR897065	2	A	CNL	SRR897458	4	A	MAY
SRR897066	2	A	CNL	SRR897459	4	A	MAY
SRR897067	2	A	CNL	SRR897460	4	A	MAY

Supplementary Table 3: (continued)

Run accession	Replicate	Sample	Center	Run accession	Replicate	Sample	Center
SRR896743	1	B	BGI	SRR897152	3	B	CNL
SRR896744	1	B	BGI	SRR897153	3	B	CNL
SRR896745	1	B	BGI	SRR897154	3	B	CNL
SRR896746	1	B	BGI	SRR897155	3	B	CNL
SRR896747	1	B	BGI	SRR897156	3	B	CNL
SRR896748	1	B	BGI	SRR897157	3	B	CNL
SRR896759	2	B	BGI	SRR897167	4	B	CNL
SRR896760	2	B	BGI	SRR897168	4	B	CNL
SRR896761	2	B	BGI	SRR897169	4	B	CNL
SRR896762	2	B	BGI	SRR897170	4	B	CNL
SRR896763	2	B	BGI	SRR897171	4	B	CNL
SRR896764	2	B	BGI	SRR897172	4	B	CNL
SRR896775	3	B	BGI	SRR897487	1	B	MAY
SRR896776	3	B	BGI	SRR897488	1	B	MAY
SRR896777	3	B	BGI	SRR897489	1	B	MAY
SRR896778	3	B	BGI	SRR897490	1	B	MAY
SRR896779	3	B	BGI	SRR897491	1	B	MAY
SRR896780	3	B	BGI	SRR897492	1	B	MAY
SRR896791	4	B	BGI	SRR897503	2	B	MAY
SRR896792	4	B	BGI	SRR897504	2	B	MAY
SRR896793	4	B	BGI	SRR897505	2	B	MAY
SRR896794	4	B	BGI	SRR897506	2	B	MAY
SRR896795	4	B	BGI	SRR897507	2	B	MAY
SRR896796	4	B	BGI	SRR897508	2	B	MAY
SRR897122	1	B	CNL	SRR897519	3	B	MAY
SRR897123	1	B	CNL	SRR897520	3	B	MAY
SRR897124	1	B	CNL	SRR897521	3	B	MAY
SRR897125	1	B	CNL	SRR897522	3	B	MAY
SRR897126	1	B	CNL	SRR897523	3	B	MAY
SRR897127	1	B	CNL	SRR897524	3	B	MAY
SRR897137	2	B	CNL	SRR897535	4	B	MAY
SRR897138	2	B	CNL	SRR897536	4	B	MAY
SRR897139	2	B	CNL	SRR897537	4	B	MAY
SRR897140	2	B	CNL	SRR897538	4	B	MAY
SRR897141	2	B	CNL	SRR897539	4	B	MAY
SRR897142	2	B	CNL	SRR897540	4	B	MAY

Supplementary Table 3: Accession information for SEQC samples.